Supplementary Information; Figures and Table

Table S1. Comparison of the NO_2 sensing capability of the Ag-functionalized SnO_2 microrods in this study to those of the previous reports.

Fig. S1 Microstructures of Ag nanoparticles synthesized with different $AgNO_3$ concentrations in γ-ray radiolysis at 10 kGy·h^{-1} for 2 h: (a) 2×10^{-2}, (b) 2×10^{-3} and (c) 2×10^{-4} mM $AgNO_3$ in a mixed solvent of deionized water (90 vol%) and 2-propanol (10 vol%).

Fig. S2 (a) Size and (b) formation density of Ag nanoparticles as a function of the precursor concentration in γ-ray radiolysis at 10 kGy·h^{-1} for 2 h.

Fig. S3 (a) X-ray photoelectron spectroscopy spectrum of the Ag-functionalized SnO_2 microrods after the heat treatment. (b) A high resolution spectrum for theAg $3d_{5/2}$ signal.

Fig. S4 Response curves of the sensors fabricated with bare and Ag-functionalized SnO_2 microrods for 1 ppm NO_2 at 300 ^{o}C during the repeated cycles.

Fig. S5 Low- and high-resolution TEM images taken from single SnO_2 microrod. The inset in the upper figure is an electron diffraction pattern taken from the microrod.

Fig. S6 Comparison of the response of the sensor fabricated with the Ag-functionalized SnO_2 microrods to those of previously reported sensors that were fabricated with different types of SnO_2 materials.

Fig. S7 Response curves of the Ag-functionalized SnO_2 microrods for 100 ppm CO, C_6H_6 and C_7H_8 at 200 ^{o}C.

Fig. S8 Energy band diagrams of the junctions (a) *p*-Ag_2O and *n*-SnO_2 and (b) Ag and *n*-SnO_2.

Table S1. Comparison of the NO_2 sensing capability of the Ag-functionalized SnO_2 microrods in this study to those of the previous reports.

Materials	NO_2 concentration (ppm)	Operating temperature (^oC)	Sensor response	Reference
Ag-functionalized SnO_2 microrod	0.1	200	780	This work
Co_3O_4-decorated ZnO nanowire	5	200	45.4	1
ZnO nanoparticles	40	290	264	2
Porous ZnO nanoflakes	0.1	175	5.6	3
Nano-tubular TiO_2	50	300	5	4
WO_3 nanorods	10	200	209	5

Reference

1 C. W. Na, H.-S. Woo, I.-D. Kim and J.-H. Lee, *Chem. Commun.*, 2011, **47**, 5148.
2 S. Bai, J. Hu, D. Li, R. Luo, A. Chen and C. C. Liu, *J. Mater. Chem.*, 2011, **21**, 12288.
3 M. Chen, Z. Wang, D. Han, F. Gu, G. Guo, *J. Phys. Chem. C*, 2011, **115**, 12763.
4 Y. Gönüllü, G. C. M. Rodríguez, B. Saruhan, M. Ürgen, *Sens. Actuators B: Chem.*, 2012, **169**, 151.
5 S. Bai, K. Zhang, R. Luo, D. Li, A. Chen and C. C. Liu, *J. Mater. Chem.*, 2012, **22**, 12643.

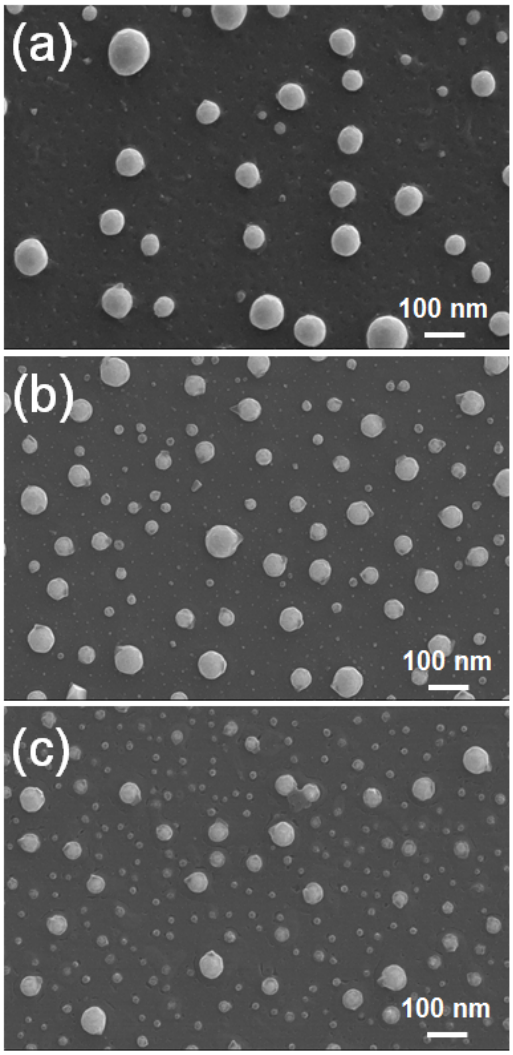

Fig. S1 Microstructures of Ag nanoparticles synthesized with different $AgNO_3$ concentrations in γ-ray radiolysis at 10 kGy·h^{-1} for 2 h: (a) 2×10^{-2}, (b) 2×10^{-3} and (c) 2×10^{-4} mM $AgNO_3$ in a mixed solvent of deionized water (90 vol%) and 2-propanol (10 vol%).

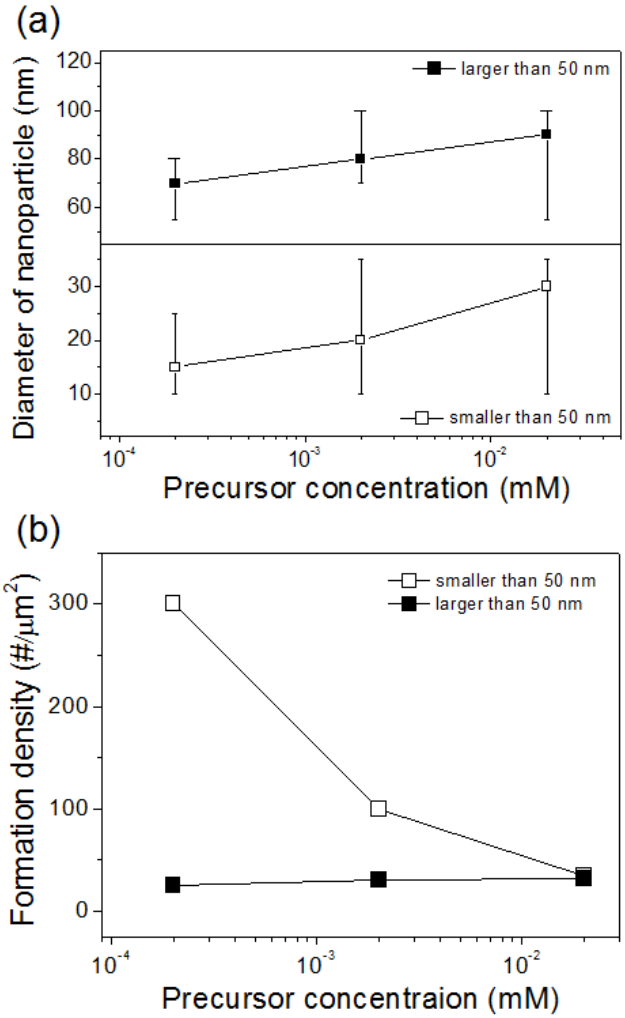

Fig. S2 (a) Size and (b) formation density of Ag nanoparticles as a function of the precursor concentration in γ-ray radiolysis at 10 kGy·h^{-1} for 2 h.

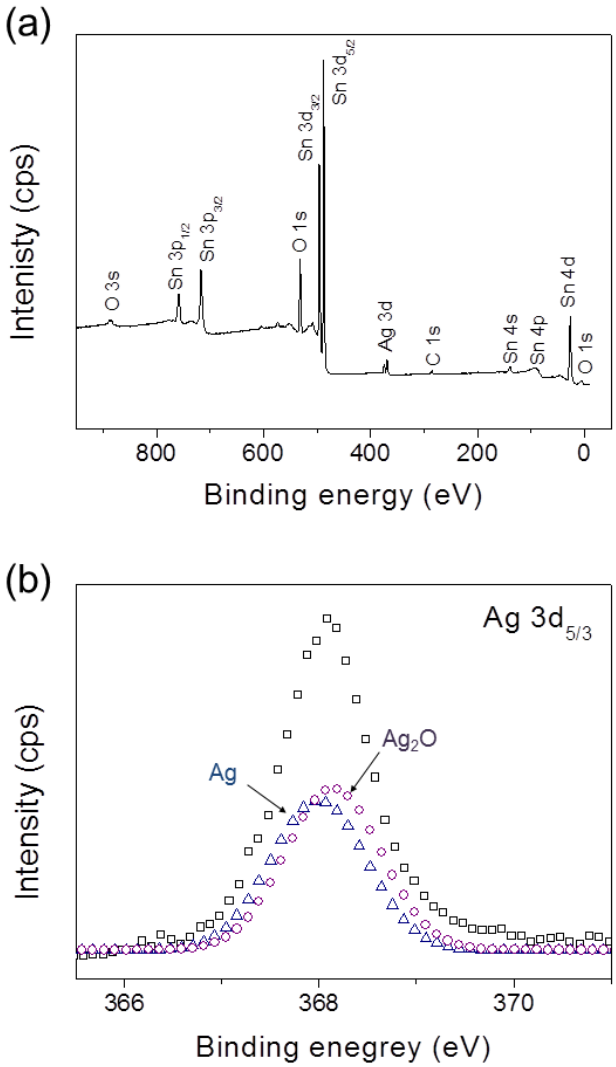

Fig. S3 (a) X-ray photoelectron spectroscopy spectrum of the Ag-functionalized SnO_2 microrods after the heat treatment. (b) A high resolution spectrum for theAg $3d_{5/2}$ signal.

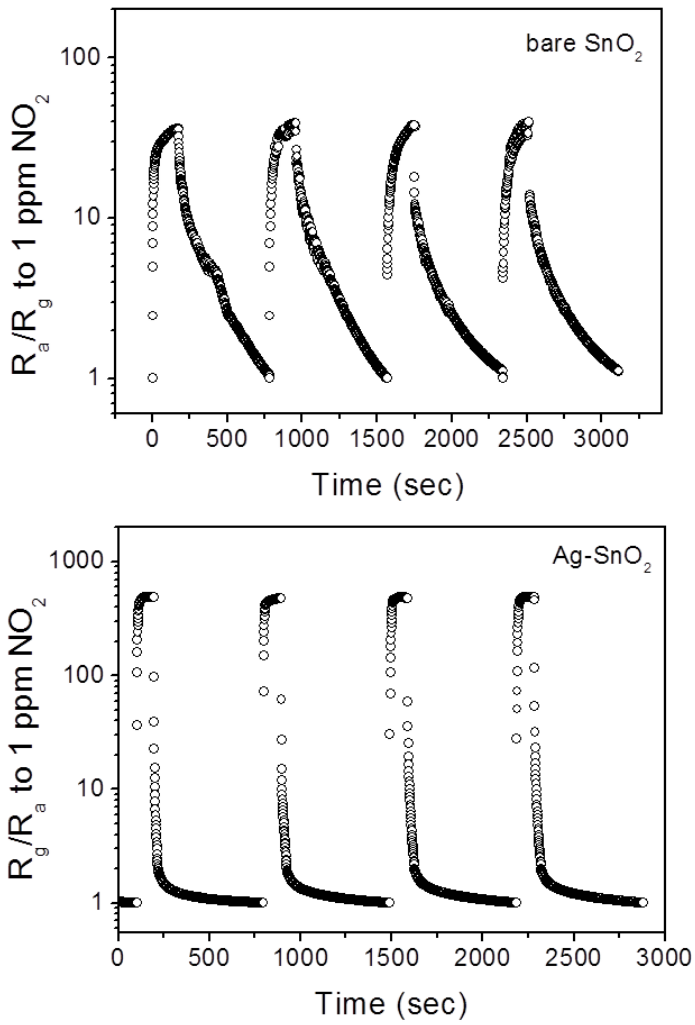

Fig. S4 Response curves of the sensors fabricated with bare and Ag-functionalized SnO_2 microrods for 1 ppm NO_2 at 300 ^{o}C during the repeated cycles.

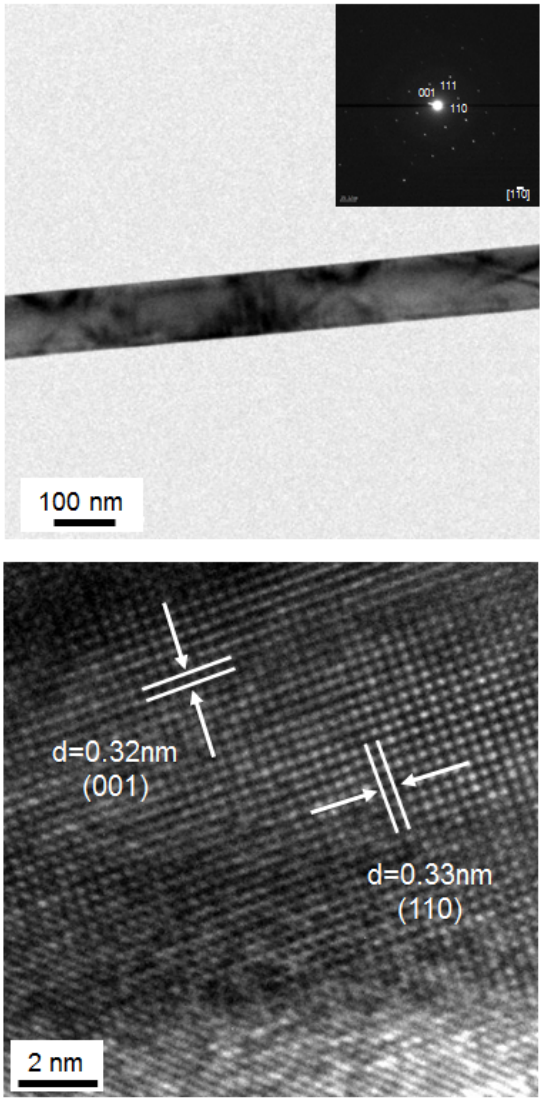

Fig. S5 Low- and high-resolution TEM images taken from single SnO_2 microrod. The inset in the upper figure is an electron diffraction pattern taken from the nanorod.

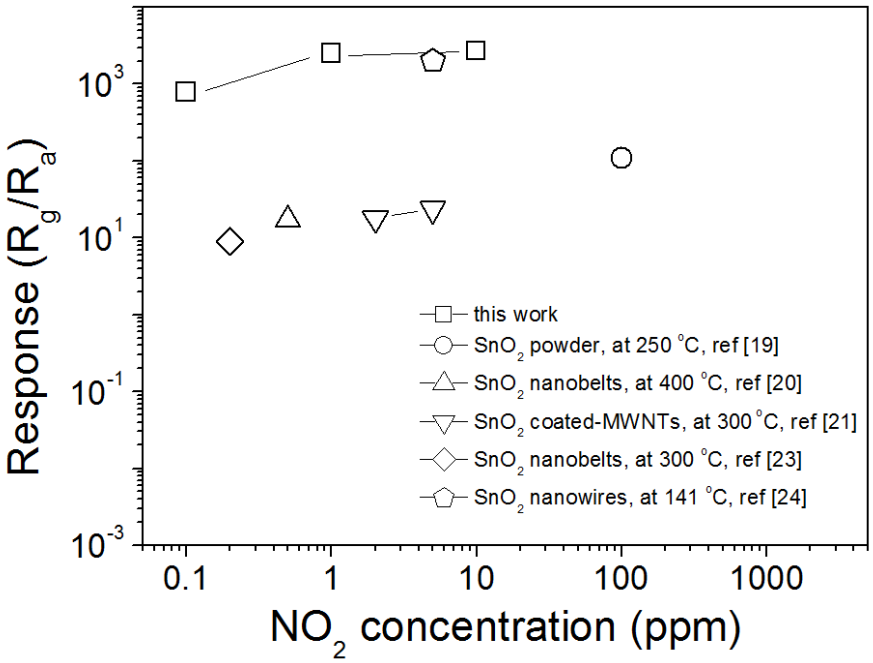

Fig. S6 Comparison of the response of the sensor fabricated with the Ag-functionalized SnO_2 microrods to those of previously reported sensors that were fabricated with different types of SnO_2 materials.

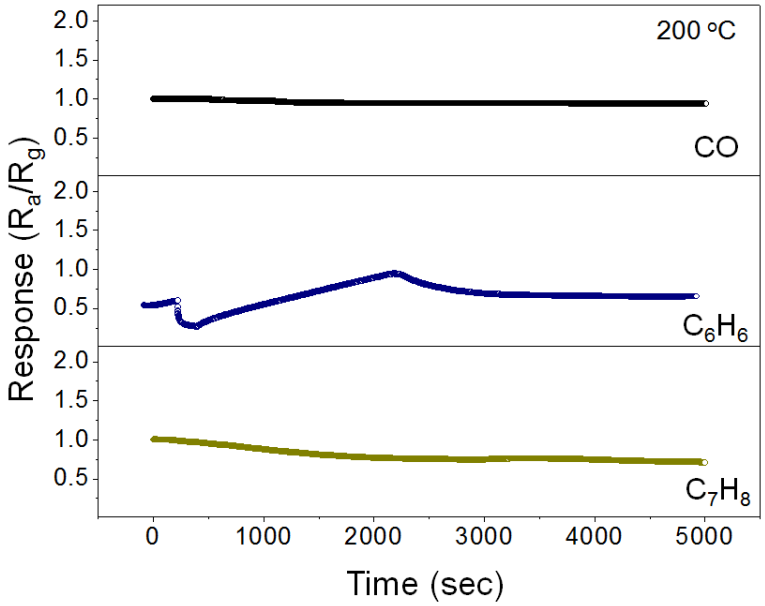

Fig. S7 Response curves of the Ag-functionalized SnO_2 nanorods for 100 ppm CO, C_6H_6 and C_7H_8 at 200 ^oC.

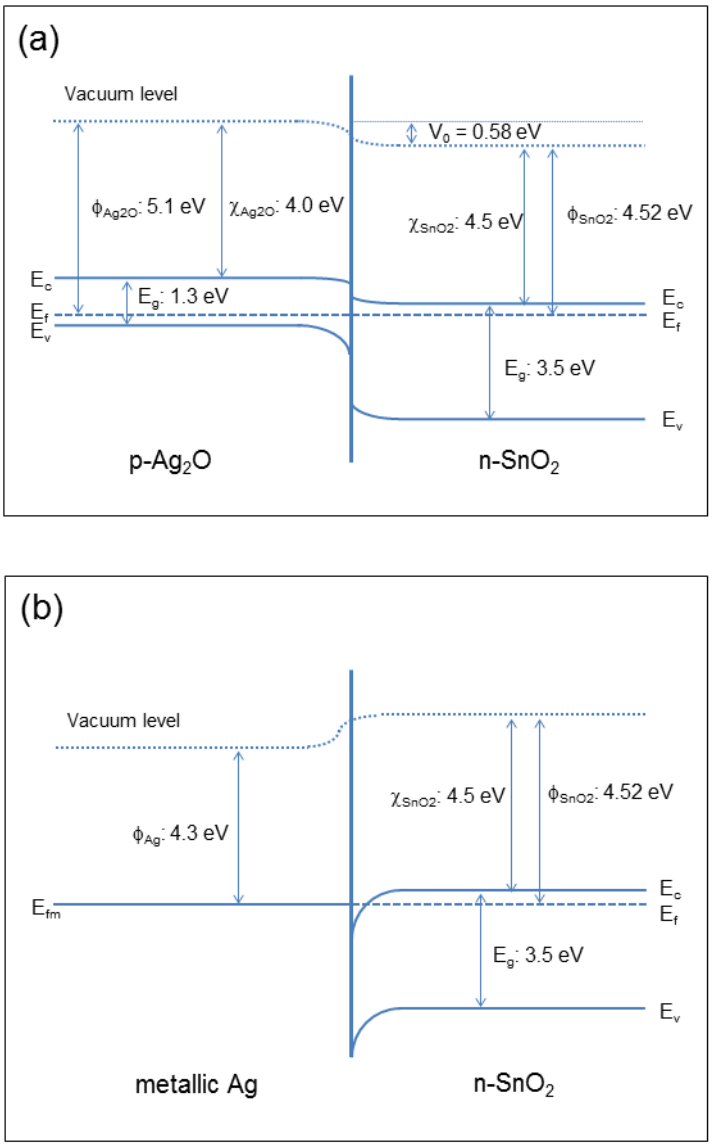

Fig. S8 Energy band diagrams of the junctions (a) *p*-Ag_2O and *n*-SnO_2 and (b) Ag and *n*-SnO_2.